ANL/ET/CP-95197

Development of Mixed-Conducting Ceramic Membranes for Hydrogen Separation *

J. Guan, S. E. Dorris, U. Balachandran
Energy Technology Division
Argonne National Laboratory
Argonne, IL 60439

M. Liu
School of Materials Science and Engineering
Georgia Institute of Technology
Atlanta, GA 30332

April 1998

Paper to be presented at the 100th Annual Meeting and Exposition of the American Ceramic Society, Cincinnati, OH, May 3-6, 1998.

*Work supported by the U.S. Department of Energy, Federal Energy Technology Center, under Contract W-31-109-Eng-38.

DISCLAIMER

DEVELOPMENT OF MIXED-CONDUCTING CERAMIC MEMBRANES FOR HYDROGEN SEPARATION

Jie Guan, Stephen E. Dorris, Uthamalingam Balachandran
Energy Technology Division, Argonne National Laboratory, Argonne, IL 60439

Meilin Liu
School of Materials Science and Engineering, Georgia Institute of Technology, Atlanta, GA 30332

ABSTRACT

$SrCeO_3$- and $BaCeO_3$-based proton conductors have been prepared and their transport properties have been investigated by impedance spectroscopy in conjunction with open circuit voltage and water vapor evolution measurements. $BaCe_{0.8}Y_{0.2}O_{3-\delta}$ exhibits the highest conductivity in a hydrogen-containing atmosphere; however, its electronic conductivity is not adequate for hydrogen separation in a nongalvanic mode. In an effort to enhance ambipolar conductivity and improve interfacial catalytic properties, $BaCe_{0.8}Y_{0.2}O_{3-\delta}$ cermets have been fabricated into membranes. The effects of ambipolar conductivity, membrane thickness, and interfacial resistance on permeation rates have been investigated. In particular, the significance of interfacial resistance is emphasized.

Keywords
Mixed conductors, hydrogen separation, transport properties, perovskites

INTRODUCTION

Mixed ionic-electronic conductors (MIECs) have been studied for application in many solid-state electrochemical systems such as solid oxide fuel cells (SOFCs), chemical sensors, and membranes for gas separation [1-7]. One well-known class of MIECs consists of partially substituted perovskite-type oxides such as $CaZrO_3$, $SrCeO_3$, and $BaCeO_3$, in which substitution of Ce or Zr by trivalent cations introduces oxygen vacancies and other charged defects and leads to mixed conduction in atmospheres containing O_2, H_2, and H_2O vapor.

These materials exhibit significant proton conduction in a hydrogen-containing atmosphere and are used for various applications. $CaZrO_3$-based ceramics are being used as a hydrogen and humidity sensor [3]; $BaCeO_3$-based prototype SOFCs are in development and significant progress has been made [4]. Meanwhile, dehydrogenation of hydrocarbons, electrolysis of steam, and pumping of hydrogen have also been demonstrated [5].

Because oxygen ion/electron conductive ceramics are being studied intensively as membranes for oxygen separation [6], it is immediately evident that dense ceramic membranes fabricated from proton/electron-conducting ceramics could also provide a simple and efficient means of separating hydrogen from gas steams and offer an alternative method of hydrogen recovery. To be suitable for hydrogen separation in a nongalvanic mode, the ceramic membranes must have sufficient protonic and electronic conductivities to achieve high permeability and selectivity to hydrogen. In addition, the materials must exhibit high catalytic activity for oxidation and evolution of hydrogen at the solid/gas interfaces.

In this study, doped $SrCeO_3$ and $BaCeO_3$ were prepared and their transport properties were investigated. Dense $BaCe_{0.8}Y_{0.2}O_{3-\delta}$ cermet membranes exhibited high hydrogen permeation rates. The dependence of permeation rate on membrane thickness and on interfacial polarization was characterized.

MEMBRANE SEPARATION MECHANISMS

In a hydrogen pump, hydrogen can be pumped by a voltage applied to the ceramic conductor from the anode to the cathode side. The hydrogen evolution rate is governed by Faraday's law, and the current efficiency depends on the transport properties of the conductor, such as the proton transference number under the operating conditions. Alternatively, hydrogen can be pumped by shorting the external circuit, where the driving force is the electrochemical potential difference across the proton conductor.

A simple and efficient approach is to use a mixed conducting membrane without electrodes. Under the conditions of ambipolar diffusion, the current density due to the motion of protons can be expressed as [8]

$$J_{H^+} = \frac{\sigma_{amb}}{L}(E_N - \eta) \qquad (1)$$

where L is the thickness of the membrane, η is the interfacial overpotential, E_N is the Nernst potential imposed across the membrane, and σ_{amb} is the ambipolar conductivity of the membrane defined as

$$\sigma_{amb} = \frac{\sigma_e \sigma_{H^+}}{\sigma_e + \sigma_{H^+}}, \quad (2)$$

if the interaction between electrons and protons is negligible. The permeation flux of hydrogen, N_{H_2}, is related to the proton current density by

$$N_{H_2} = \frac{J_{H^+}}{2F}. \quad (3)$$

It is clear that the permeation flux of hydrogen through the MIEC membrane can be improved by enhancing of ambipolar conductivity and reducing of the membrane thickness and interfacial overpotential.

The interfacial overpotential η and ambipolar conductivity σ_{amb} can be determined by measuring permeation rates through membranes with different thicknesses. If Eqs. 1 and 3 are rewritten as [9]

$$\frac{E_N}{2FN_{H_2}} = \frac{\eta}{2FN_{H_2}} + \frac{L}{\sigma_{amb}}, \quad (4)$$

then the interfacial polarization resistance, R_p, can be estimated from

$$R_p = \left(\frac{E_N}{2FN_{H_2}} \right)_{L \to 0}, \quad (5)$$

while ambipolar conductivity can be determined as

$$\sigma_{amb} = \left[\frac{\partial \left(E_N / 2FN_{H_2} \right)}{\partial L} \right]^{-1}. \quad (6)$$

EXPERIMENTAL

Sample Preparation

$SrCeO_3$-and $BaCeO_3$-based ceramic powders and pellets were prepared as described in Refs. 10 and 11. Pt paste was applied to polished surfaces of the pellets and fired in air at 1200°C for 12 min to form porous electrodes before electrochemical characterization. Cermet membranes were prepared by mixing metallic powder with $BaCe_{0.8}Y_{0.2}O_{3-\delta}$. After being ball-milled for 24 h, the resulting powders were pressed at 200 MPa and then sintered at 1400°C for 5 h in 4% H_2 balance argon.

Impedance Spectroscopy

The ceramic pellets with two Pt electrodes were immersed in various atmospheres at different temperatures (600-800°C). Total conductivity was measured with an impedance analyzer (HP 4192A) in the frequency range of 13

MHz to 5 Hz under open-circuit conditions. Water vapor was introduced by bubbling desired gases through deionized water at room temperatures.

Ionic Transference Numbers

Transference numbers were determined by measuring either open-circuit voltage (OCV) or water vapor evolution rates. OCVs of fuel cells and concentration cells, measured by a high-impedance digital multimeter (HP 3446A), were used to estimate the ionic and electronic transference numbers. The ionic transference numbers so obtained may be underestimated in some cases because of interfacial polarization [12]. Evolution of water vapor by discharging an O_2/H_2 fuel cell was used to determine the ratio of proton and oxide ion transference numbers to the total ionic transference numbers. The gas inlets in the setup were positioned as close as possible to the test sample. Gas flow rates were adjusted to 50-100 cm^3/min. Water vapor concentration in both cathode and anode sides was measured with a digital hygrometer (Fisher Scientific) under open- and short-circuit conditions.

Hydrogen Pumping and Water Vapor Electrolysis

A 2.09-mm-thick pellet of $BaCe_{0.8}Y_{0.2}O_{3-\delta}$ with three electrodes was affixed to a test setup (Fig. 1) with a glass sealant. Hydrogen was pumped from the anodic to the cathodic side by applying a constant DC current. The anodic side was fed with 4% H_2 balance N_2 at 86 cm^3/min and the cathodic side was swept by Ar at 43 cm^3/min. The anodic overpotentials were directly determined by measuring the potentials between the anode and the reference electrode. In water vapor electrolysis, Ar saturated with water vapor at room temperature was fed to the anode side at 86 cm^3/min, and the cathode side was also swept with Ar at 43 cm^3/min. Gas concentrations were analyzed with a gas chromatograph (HP 5830A) and a hygrometer.

Hydrogen Permeation through Cermet Membranes

Polished cermet membranes with three different thicknesses (0.095, 0.114, and 0.205 cm) were also affixed with a glass sealant to one end of Al_2O_3 tubes, as illustrated in Fig. 2. The effective membrane area for permeation was 1.4 cm^2. A sample gas (4% H_2 balance Ar) was fed to one side at a rate of 86 cm^3/min, while a carrier gas (Ar) was swept to the opposite side of the membrane at a rate of 43 cm^3/min. The gas concentrations were analyzed with a gas chromatograph that was periodically calibrated with a standard gas. Gas leakage through the setup

was tested with helium as the feeding gas; typical leakage was <10% of the total permeation flux.

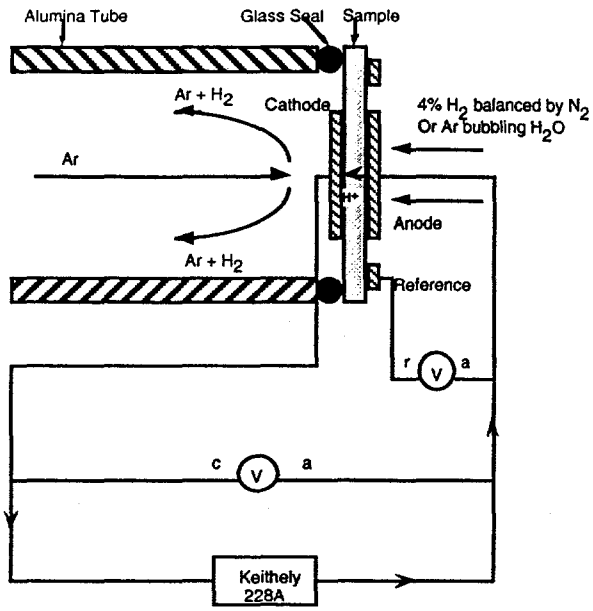

Fig. 1 Schematic illustration of hydrogen pumping and water vapor electrolysis.

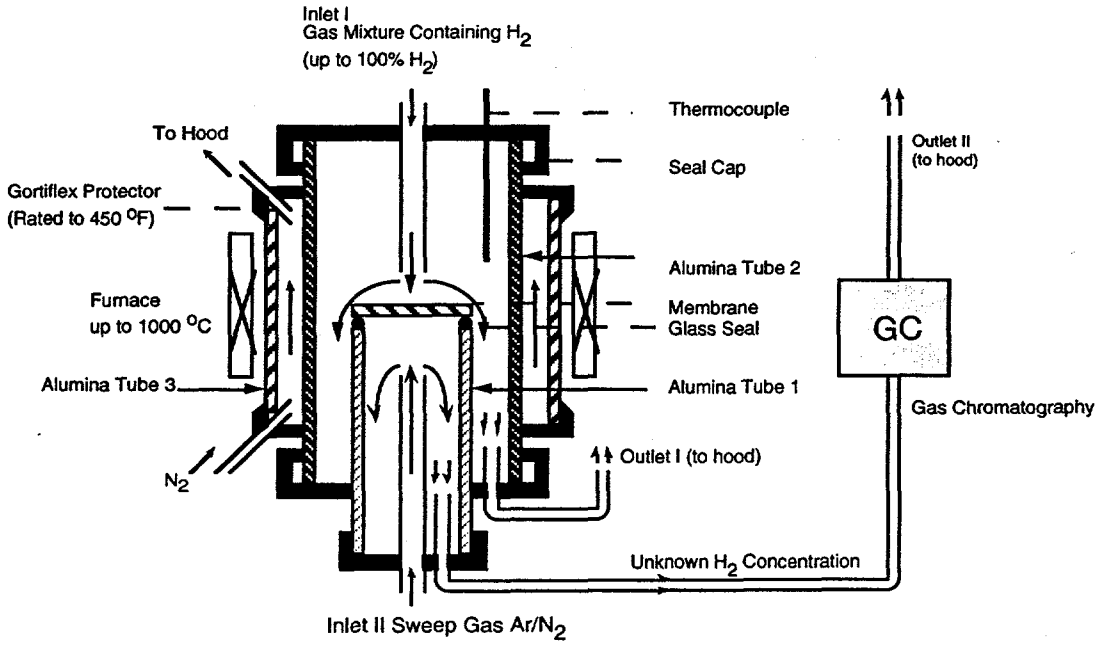

Fig. 2 Schematic illustration of setup for hydrogen separation.

RESULTS AND DISCUSSION

Conductivity

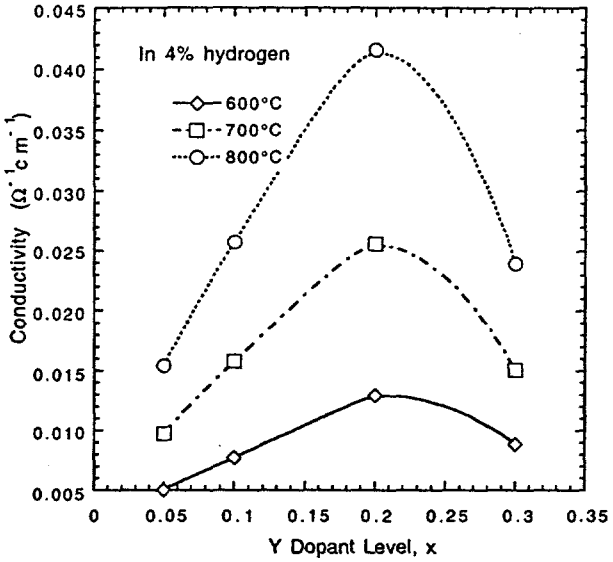

Fig. 3 Conductivity of $BaCe_{1-x}Y_xO_{3-\delta}$ in 4% hydrogen at various temperatures.

$BaCeO_3$-based materials exhibit higher total conductivities than $SrCeO_3$-based materials in both hydrogen and oxygen [11]. Conductivity of $BaCe_{1-x}Y_xO_{3-\delta}$ varied with the doping concentration x (Fig. 3). At a given temperature, conductivity measured in 4% H_2, which is dominated by ionic conduction, increased monotonically with dopant concentration from $x = 0.05$ to 0.2, then decreased for an Y-concentration of 0.3, suggesting that the conductivity in hydrogen reached its maximum at $0.2 \leq x < 0.3$. The increase in conductivity with dopant concentration could be related to an increase in charge carrier concentration through the reaction

$$Y_2O_3 \xrightarrow{CeO_2} 2Y'_{Ce} + 3O_O^{\times} + V_O^{\bullet\bullet} \qquad (7)$$

in the solubility limit. The decrease in conductivity for $x > 0.2$ was probably contributed to phase segregation when the solubility limit of Y was reached.

Ionic Transference Numbers

The proton transference number of Y-doped $SrCeO_3$ and $BaCeO_3$ materials was estimated to be about 0.8-0.95 from a hydrogen concentration cell in the

temperature range of 600-800°C. The ratios of proton and oxide ion transference numbers to total ionic transference numbers were further studied with a fuel cell of

$$100\%\ O_2,\ Pt \mid SrCe_{0.95}Y_{0.05}O_{3-\delta} \mid Pt,\ 4\%\ H_2 + Ar. \qquad (8)$$

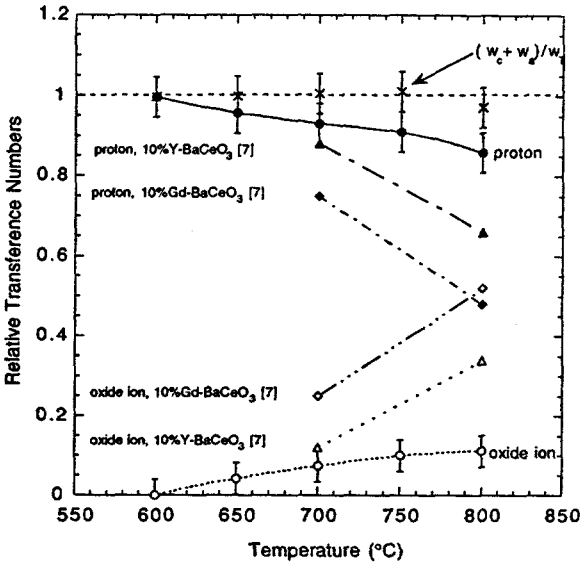

Fig. 4 Ratios of proton and oxygen ion transference number to total ionic transference number in $SrCe_{0.95}Y_{0.05}O_{3-\delta}$ and in $BaCeO_3$-based materials [7].

When the two electrodes are set at equal potentials, the current that passes through the electrolyte is approximately ionic, while electronic current is negligible. Accordingly, the ratios of (t_{H^+}/t_{ion} and $t_{O^{2-}}/t_{ion}$) can be determined as follows:

$$\frac{t_{H^+}}{t_{ion}} = \frac{w_c}{w_t}, \qquad (9a)$$

$$\frac{t_{O^{2-}}}{t_{ion}} = \frac{w_a}{w_t}, \qquad (9b)$$

and

$$t_{ion} = t_{H^+} + t_{O^{2-}}, \qquad (9c)$$

where w_c and w_a are the rates of water vapor evolution from the cathode and anode sides, respectively, and w_t is the total rate of water vapor evolution from both sides or the total rate of water evolution calculated from the short-circuit currents (when Faraday's law is applied). The rates of water vapor evolution due to the electrochemical process were calculated from the flow rates of carrier gas

and humidity measured in both sides of the cell under open- and short-circuit conditions. The rate of water vapor evolution from the anode side (hydrogen side) was much slower than that from the cathode side (oxygen side), indicating that proton transport dominated the ionic transport. The total rate of water vapor evolution observed on both sides was in very good agreement with the rate calculated from short-circuit currents. As shown in Fig. 4, the ionic transference numbers are dominated by protons, even at 800°C. Unlike $BaCeO_3$-based materials [13], $SrCe_{0.95}Y_{0.05}O_{3-\delta}$ did not exhibit a conduction transition from proton to oxide ion as temperature increased from 600-800°C. In the temperature range studied, proton transference numbers were much higher than oxide ion transference numbers.

Hydrogen Pumping and Water Vapor Electrolysis

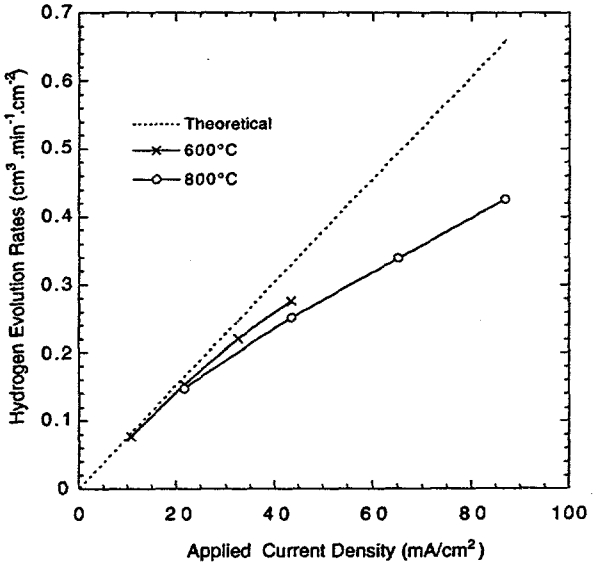

Fig. 5 Hydrogen pumping rates as a function of current density and temperatures.

Shown in Fig. 5 are the hydrogen evolution rates as a function of applied currents and temperatures. The theoretical values calculated from Faraday's law are also shown for reference. When the applied current was low (<22 mA/cm^2), the current efficiency was close to unity, which was in good agreement with the high proton transference numbers of the materials (0.8-0.95). Current efficiency dropped significantly at higher current densities, and this was more evident at high temperature (800°C) than at low temperature (600°C).

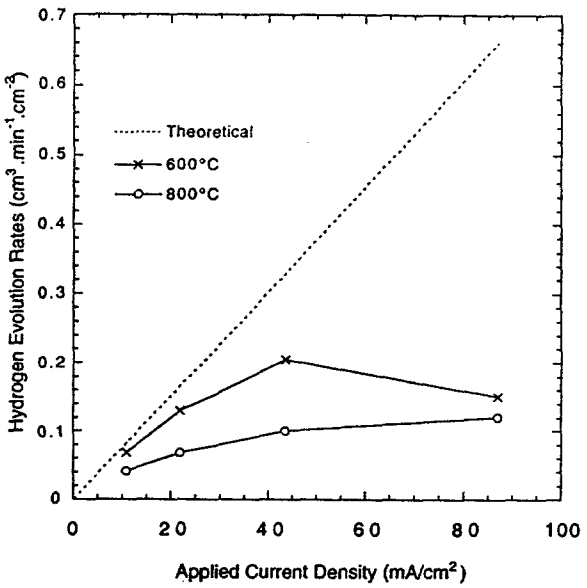

Fig. 6 Hydrogen evolution rates during water vapor electrolysis.

Very dry hydrogen (dew point < -40°C) was obtained by electrolyzing water vapor. As shown in Fig. 6, the current efficiencies were lower than those observed in hydrogen pumping. The low current efficiencies suggested that oxygen ion and electron conduction was significant in water vapor electrolysis. Electron holes could have been formed in a reaction of the oxygen vacancies with the oxygen, which may remains locally at the anodic interface with a relatively higher pressure as a by-product of the water vapor electrolysis:

$$\frac{1}{2}O_2 + V_O^{\bullet\bullet} \rightarrow O_O^{\times} + 2h^{\bullet}. \qquad (10)$$

Hydrogen Permeation through Cermet Membranes

Figure 7 shows net permeation flux through three cermet membranes. Hydrogen permeation rates increased with temperature and were approximately proportional to the inverse of membranes thickness (0.095 to 0.205 cm) at high temperature (800°C), with a slope close to $(E_N\sigma_{amb})/2F$. This suggests that the rate-limiting step is the bulk properties for samples with thicknesses between 0.095 and 0.205 cm. However, at low temperatures (<650°C), the flux data showed significant deviation from this relationship, suggesting that interfacial resistance, rather than bulk properties, is significant at low temperatures.

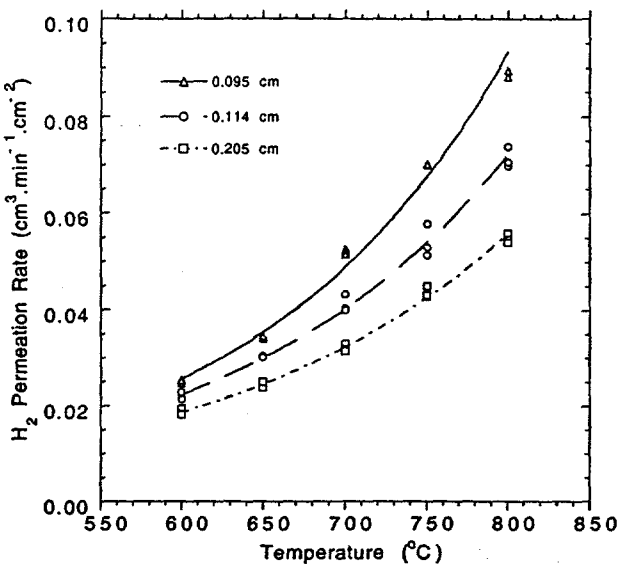

Fig. 7 Temperature and thickness dependence of hydrogen permeation rates through $BaCe_{0.8}Y_{0.2}O_{3-\delta}$ cermet membranes.

Significance of Interfacial Polarization

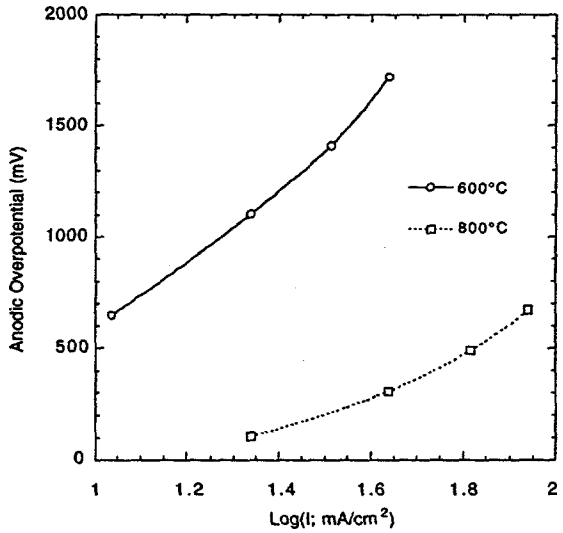

Fig. 8 Anodic overpotentials as a function of applied current density during hydrogen pumping.

As shown in Fig. 8, significant anodic overpotentials were observed in hydrogen pumping, which consumed about 50-70% of the applied potentials under the pumping conditions studied. Interfacial polarization resistances of cermet membranes were investigated through dependence of the gas permeation rate on membrane thickness, as implied by Eq. 5. The interfacial polarization resistance declined dramatically with an activation energy of about 1.03 eV when temperature was increased from 600 to 800°C (Fig. 9). At high temperature (800°C), bulk resistance is much greater than interfacial resistance when sample thickness is >0.095 cm; at lower temperatures, however, interfacial resistance is likely predominant. Thus, reducing the membrane thickness will enhance the permeation flux significantly only if the bulk transport properties are more important than interfacial polarization.

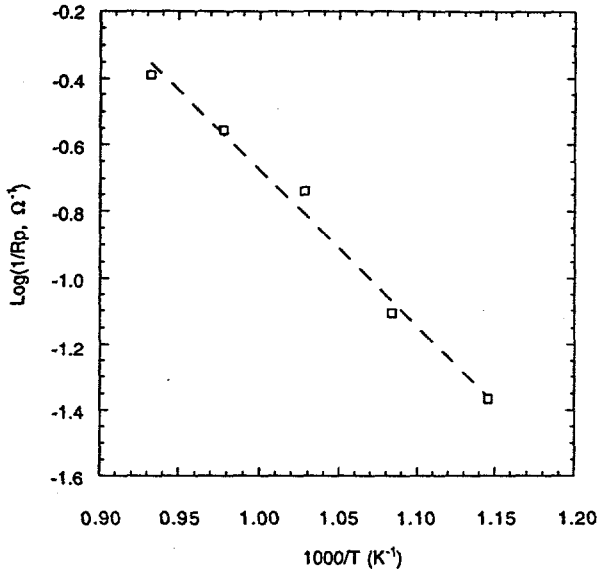

Fig. 9 Interfacial resistance of $BaCe_{0.8}Y_{0.2}O_{3-\delta}$ cermet membrane (1.4 cm^2 in area) as a function of temperature.

CONCLUSIONS

$SrCeO_3$- and $BaCeO_3$-based materials are good proton conductors in hydrogen-containing atmospheres. Hydrogen was pumped though $BaCe_{0.8}Y_{0.2}O_{3-\delta}$ by a DC current; the current efficiency decreased with an increase in temperature and applied current density. Significant interfacial polarization was observed and further reduced the energy efficiency in hydrogen pumping and steam electrolysis.

$BaCe_{0.8}Y_{0.2}O_{3-\delta}$ cermets can be used as MIEC membranes for hydrogen separation in a nongalvanic mode. Interfacial resistances were significant at low temperatures. Further reduction of membrane thickness may not improve the permeation rate effectively if interfacial polarization is more significant than bulk resistance.

ACKNOWLEDGMENTS

This work has been supported by the U.S. Department of Energy, Federal Energy Technology Center, under Contract W-31-109-Eng-38

REFERENCES

[1]. N.Q. Minh and T. Takahashi, "Science and Technology of Ceramic Fuel Cells," Elsevier Science, Amsterdam, 1995.

[2]. H.J.M. Bouwmeester and A.J. Burggraaf, in: Fundamentals of Inorganic Membrane Science and Technology, A.J. Burggraaf and L. Cot, eds., Elsevier Science, Amsterdam, 435 (1996).

[3]. N. Fukatsu, N. Kurita, T. Yajima, K. Koide, and T. Ohashi, J. Alloys and Comp., **231**, 706-12 (1995).

[4]. N. Taniguchi, E. Yasumoto, T. Gamo, J. Electrochem. Soc., **143**, 1886 (1996).

[5]. J. Langguth, R. Dittmeyer, H. Hofmann, and G. Tomandl, Chemie Ingenieur Technik, **69**, 3197 (1997).

[6]. U. Balachandran, J.T. Dusek, S.M. Sweeney, R.B. Poeppel, R.L. Mieville, P.S. Maiya, M.S. Kleefisch, S. Pei, T.P. Kobylinski, C.A. Udovich, and A.C. Bose, Am. Ceram. Soc. Bull., **74**, 71 (1995).

[7]. H. Iwahara, T. Yajima, and H. Uchida, Solid State Ionics, **70/71**, 267 (1994).

[8]. M. Liu, Proc. 1st Int. Symp. on Ionic and Mixed Conducting Ceramics, T. A. Ramanarayana and H. L. Tuller, eds., The Electrochemical Society, Pennington, NJ, Vol. **91-12**, 215 (1991).

[9]. M. Liu and A. Joshi; 1st Int. Symp. on Ionic and Mixed Conducting Ceramics, T. A. Ramanarayana and H. L. Tuller, eds., The Electrochemical Society, Pennington, NJ, Vol. **91-12**, 231 (1991).

[10]. J. Guan, S. E. Dorris, U. Balachandran, and M. Liu, Solid State Ionics, **100**, 45 (1997).

[11]. J. Guan, S. E. Dorris, U. Balachandran, and M. Liu, J. Electrochem. Soc., **145**, 1780 (1998).

[12]. M. Liu and H. Hu, J. Electrochem. Soc. **143**, L109 (1996).

[13]. N. Bonanos, K. S. Knight, and B. Ellis, Solid State Ionics, **79**, 161 (1995).